ACS OMEGA

Open Access

http://pubs.acs.org/journal/acsodf

Article

Nanoassembly-Mediated Exendin-4 Derivatives to Decrease Renal Retention

Zhengwei Zhou, Shuai Wang, Tianling Feng, Pengjun Zhang, Hongwei Fan,* Jianjun Zou,* and Kaizong Huang*

Cite This: *ACS Omega* 2024, 9, 18757−18765

Read Online

ACCESS | Metrics & More | Article Recommendations | Supporting Information

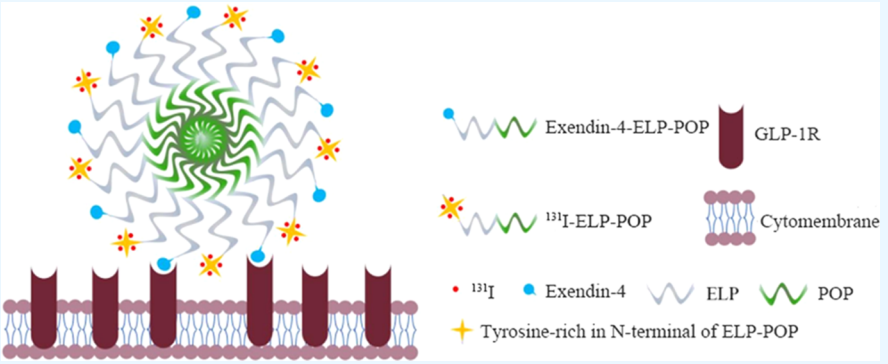

ABSTRACT: An Exendin-4 analogue that was conjugated with ^{68}Ga exhibited an excellent diagnostic effect on insulinoma in clinical practice. On account of its low molecular weight and short hydration radius, ^{68}Ga-Exendin-4 showed high accumulation in kidney tissues. Nanoparticle-mediated strategies have attracted much attention due to polyvalent properties and the size amplification effect. In this study, Exendin-4 derivatives of radionuclide nanodevices were developed and evaluated. The Exendin-4 derivatives consisting of a ternary block recombinant protein were purified by an inverse transition cycle (ITC) and allowed to self-assemble into a nanodevice under physiological conditions. Our results showed that the nanoassemblies of Exendin-4 derivatives formed homogeneous spherical nanoparticles, exhibited outstanding affinity for insulinoma cells, and could be deposited in insulinoma tissues *in vivo*. The nanoassembly-mediated Exendin-4 derivatives showed fivefold reduced renal retention and exhibited an outstanding tumor-suppression effect.

1. INTRODUCTION

Insulinoma is a functional pancreatic neuroendocrine tumor that originates from pancreatic β-cells. Studies have shown that glucagon-like peptide-1 receptor (GLP-1R) is highly expressed on the surface of insulinoma cells, and GLP-1R targeting imaging technology had been applied to diagnose insulinoma in clinical practice.[1] Targeting GLP-1R with indium-111-, technetium-99m-, or gallium-68-labeled Exendin-4 offers a new approach that permits successful localization of insulinomas.[2] In our previous study, a GLP-1 analogue (Exendin-4) that was conjugated with ^{68}Ga (^{68}Ga-Exendin-4) provided an outstanding diagnosis for insulinoma.[3] However, on account of its low molecular weight and short hydrated radius, ^{68}Ga-Exendin-4 presented high accumulation in the kidney tissues, which caused radiation damage and thus limited clinical application.

Several strategies for reducing the renal accumulation of radiolabeled Exendin-4 derivatives have been exploited. For example, the coadministration of basic amino acids or the introduction of a cleavable linker into Exendin-4 derivatives has been examined *in vivo*.[4] Unfortunately, these strategies did not brought about higher accumulation in tumors.[5]

Particles with a diameter smaller than 5−6 nm are rapidly cleared by the kidney (half-life, <600 min in the blood), while increasing particle diameter can significantly enhance the half-life of agents in the blood and body.[6−8] We demonstrated that self-assembling diblock elastin-like polypeptides (ELPs) conjugated with an agent could overcome the limitation of accumulation in the kidney and bladder.[9,10] The diblock ELP could self-assemble into a nanoparticle, thereby increasing the hydraulic radius of the nanodevice and effectively avoiding clearance by the kidney. Accumulating reports have implicated that a polyalanine domain insert into hydrophobic ELP (partially ordered polymers were named POP) could achieve greater stability in the fomulation of nanoassemblies.[11]

Received: July 12, 2023
Revised: October 16, 2023
Accepted: October 24, 2023
Published: April 21, 2024

In this study, we proposed novel nanoassembly-mediated Exendin-4 derivatives, which consist of Exendin-4 blocks, hydrophilic ELP blocks, and hydrophobic POP blocks. It was expected that amphiphilic Exendin-4-ELP-POP could form nanoassemblies under physiological conditions and effectively reduce kidney and bladder aggregation.[12] In addition, the formulation of Exendin-4-ELP-POP nanoassemblies showed that the GLP-1 block emerged on the surface at high density and implemented multivalent binding. An ^{131}I-ELP-POP molecule was generated by conjugating ^{131}I with the tyrosine-rich N-terminus of ELP-POP.[13,14] Owing to the extremely similar structures between ^{131}I-ELP-POP and Exendin-4-ELP-POP, it was estimated that the combination of ^{131}I-ELP-POP and Exendin-4-ELP-POP generated homogeneous nanoassemblies at physiological temperatures and yielded a significant therapeutic effect on insulinoma.

2. MATERIALS AND METHODS

2.1. Materials. Rat islet tumor cells (INS-1) and their medium were purchased from Procell Ltd., Corp. (Wuhan China), and CCK-8 (cell counting kit-8) was supplied by Beyotime Biotechnology Ltd., Corp. Peptone and yeast extract were purchased from Oxoid Ltd., Corp. Other chemical agents were obtained from Sigma Ltd., Corp.

2.2. Construct Exendin-4-ELP-POP Expression Vector. The plasmid construction was performed using our previously published method.[10] The hydrophilic ELP block (ELP-[$V_1A_7G_8$-48]) contains three ELP[$V_1A_7G_8$-16] repeats, each containing 16 VPGXG pentapeptides, in which the fourth variable amino acid X is composed of valine (*V*), alanine (A), and glycine (G), with a composition ratio of V:A:G = 1:7:8. The hydrophobic POP block is composed of three repeat units $VPGVG_{15}$-A_{25}, which encodes 15 VPGVG pentapeptide repeats and 25 alanine amino acid residues. The correct encode sequence was ensured by enzyme digestion and sequencing. The 17 tyrosine residues or the Exendin-4 block was fused with the ELP[$V_1A_7G_8$-48] block and the POP block, defined as ELP-POP and Exendin-4-ELP-POP, respectively.

2.3. Expression, Purification, and Identification of Exendin-4-ELP-POP. The recombination protein expression of Exendin-4-ELP-POP was induced overnight at 37 °C and purified by an inverse transition cycle (ITC). After three rounds of ITC purification, the proteins were freeze-dried and were ready for further use.

2.4. Thermal Characterization. Exendin-4-ELP-POP and ELP-POP powder were dissolved in PBS at a concentration of 100 μmol/L. The optical density at 350 nm was recorded in the range from 15 to 45 °C at a heating rate of 1 °C/min. The transition temperature (Tt) was determined from the midpoint of the maximum of the turbidity gradient.

2.5. Nanoassemblies' Formation and Particle Size Determination. Recombinant protein was dissolved in PBS to obtain a final concentration of 100 μmol/L protein solution. The recombinant protein was incubated at 37 °C for 10 min to induce micellar formation. The hydrated particle size of the nanoassemblies was measured by dynamic light scattering (DLS) at 37 °C. To further verify the size of the nanoassemblies, the morphology of Exendin-4-ELP-POP and ELP-POP was captured by the JEM-1010 transmission electron microscope (TEM). Zeta potential was recorded by a particle size analyzer (Malvern).

2.6. Synthesis of Cy5-Labeled Recombinant Protein. Cy5 containing a succinamide ester group could react with amino groups. Cy5 fluorescent dye was added to 5 mL of PBS solution containing 100 μmol/L Exendin-4-ELP-POP or ELP-POP, and the reaction was kept in the dark for 4 h at 4 °C. Subsequently, the reagent was placed at 4 °C for dialysis overnight to remove free Cy5.

To test the affinity ability, the cells were incubated with Cy5-labeled recombinant protein for 2 h at 37 °C. Images were obtained using confocal laser microscopy.

2.7. CCK-8 Assay Toxicity of ^{131}I-Labeled ELP-POP and Combination of Exendin-4-ELP-POP with ELP-POP. Rat islet tumor cells (INS-1) were seeded in 96 wells (5000 cells in 200 μL per well) and allowed to adhere. Cells were then recultivated in fetal bovine serum-free medium added with free ^{131}I, ^{131}I-ELP-POP, and combination of Exendin-4-ELP-POP with ^{131}I-ELP-POP at different concentrations (0, 1.85, 3.7, 18.5 MBq/mL) for 24 h at 37 °C. INS-1 cells' viability was determined by the CCK-8 assay following the manufacturer's method.

2.8. *In Vivo* Fluorescence Imaging. INS-1 (logarithmic growth stage) was harvested, and then PBS was added to adjust the cell suspension with a concentration of 5×10^7/mL. Cell suspension (100 μL) was injected subcutaneously into the right side of each BALB/c nude mouse. Female athymic nude mice bearing a subcutaneously implanted insulinoma (approximately 350−500 mm^3) were anesthetized by inhalation and intravenously injected with Cy5-labeled recombinant protein nanoassembly formulation. *In vivo* fluorescence imaging was performed by scanning the mouse abdomen at predetermined time intervals using a Lumina XR system (Caliper, Life science). At 48 h post injection, the mice were anesthetized and sacrificed. Representative organs and tumor were harvested. Each organ and tumor were rinsed with saline three times and put into the board. The region-of-interest (ROI) function of the analysis workstation software was used to calculate the fluorescence distribution of the three groups of mice. The quantification of fluorescent signals was performed as total photons per centimeter squared per steradian (p/s/cm^2/sr) per organ and tumor.

2.9. Radiotherapy Effect *In Vivo*. Radiolabeling of ELP-POP with ^{131}I was performed by the chloramine-T method following a previous report.[14] Briefly, ELP-POP was dissolved in cold PBS (100 μmol/L) and added with 20 mCi (740 MBq) ^{131}I-sodium−iodine and chloramine-T. The mixture was stirred and incubated for 2 h at 4 °C and then subjected to dialysis for 18 h to remove free ^{131}I. The labeling rate and purity were evaluated by radiation intensity, and the iodine molecule labeling efficiency was analyzed by MALDI-TOF.

Female athymic nude mice bearing a subcutaneous insulinoma (80−100 mm^3) were randomly divided into four groups, with three mice in each group. 13.7 MBq radiation dose drug was administered by IV injection. The tumor and body weight were measured every three days until the tumor reached the maximum ethically required loading volume (1500 mm^3). The calculation formula of tumor volume for mice is $V = (L \times W^2)/2$, where *L* is the long diameter and *W* is the short diameter of the tumor.

2.10. Statistical Analysis. Statistical comparisons were performed by one-way ANOVA for multiple groups, and *p* values <0.05 and <0.01 were considered indications of a statistical difference and a statistically significant difference, respectively.

https://doi.org/10.1021/acsomega.3c04644
ACS Omega 2024, 9, 18757−18765

3. RESULTS

3.1. Recombinant Protein Purification. As Figure S1 shows, the plasmid that contains Exendin-4-ELP-POP and ELP-POP genes, respectively, was successfully constructed and further verified by sequencing. The recombination protein expression was induced and purified by ITC.[4] ELP-POP and Exendin-4-ELP-POP could highly be expressed by the soluble form (Figure 1, Lane1 and Lane2), and its purity gradually increased by using ITC (Figure 1, Lane 3 and Lane 4). After purification of the recombination protein by three rounds of ITC, a single, bright band was obtained at a molecular weight of approximately 47 kDa, consistent with the theoretical molecular weight of ELP-POP (Figure 1, Lane 5). Similarly, Exendin-4-ELP-POP was also purified by ITC (Figure 1, Lane 6).

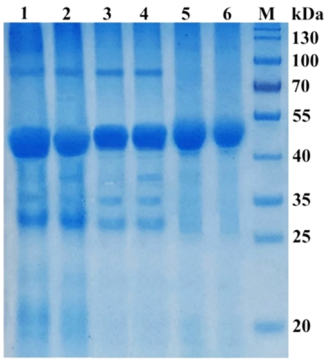

Figure 1. SDS-PAGE analysis of Exendin-4-ELP-POP and ELP-POP; Lane M, Marker; Lane1, ELP-POP bacterial lysate; Lane2, Exendin-4-ELP-POP bacterial lysate; Lane3, supernatant of bacterial solution after ELP-POP centrifugation; Lane4, supernatant of bacterial solution after centrifugation with Exendin-4-ELP-POP; Lane5, ELP-POP after three rounds of ITC purification; Lane6, Exendin-4-ELP-POP after three rounds of ITC purification.

3.2. Characterization of Exendin-4-ELP-POP and ELP-POP. The optical absorbance at 350 nm of Exendin-4-ELP-POP and ELP-POP was recorded at varying temperatures from 15 to 45 °C. Transition temperature was defined as the solution temperature at the maximum of the turbidity gradient. We estimated that the transition temperatures were 38.5 and 39.1 °C, pointing to Exendin-4-ELP-POP and ELP-POP, respectively (Figure S2).

The amphiphilic recombinant protein designed in this study can form nanoassemblies under physiological conditions. The dynamic light scattering result displayed that the nanoassemblies formed by Exendin-4-ELP-POP and ELP-POP were homogeneous in distribution, with a hydraulic diameter of ∼100 nm [Figures 2(a) and S3]. TEM results demonstrated that they formed homogeneous spherical nanoassemblies with a particle size of ∼100 nm. Additionally, similar sizes were observed between Figure 2(d),2(e), which correspond to ELP-POP and the combination of Exendin-4-ELP-POP with ELP-POP. These results indicate that the Exendin-4 block had minimal effect on the ELP-POP nanostructure. The ζ potentials of Exendin-4-ELP-POP, ELP-POP, and the combination of Exendin-4-ELP-POP with ELP-POP were 10.05, −5.76, and −8.35 mV, respectively.

3.3. High Affinity of Exendin-4-ELP-POP for Insulinoma Cells. As shown in Figure 3, in terms of the Cy5-Exendin-4-ELP-POP group, the red fluorescent signal of the group indicated more aggregation on the membrane of INS-1. In contrast, a weak red fluorescent signal appeared in the Cy5-ELP-POP group. The combination of Cy5-Exendin-4-ELP-POP with ELP-POP group emerged to have a similar targeting property to the Cy5-Exendin-4-ELP-POP group; this indicated

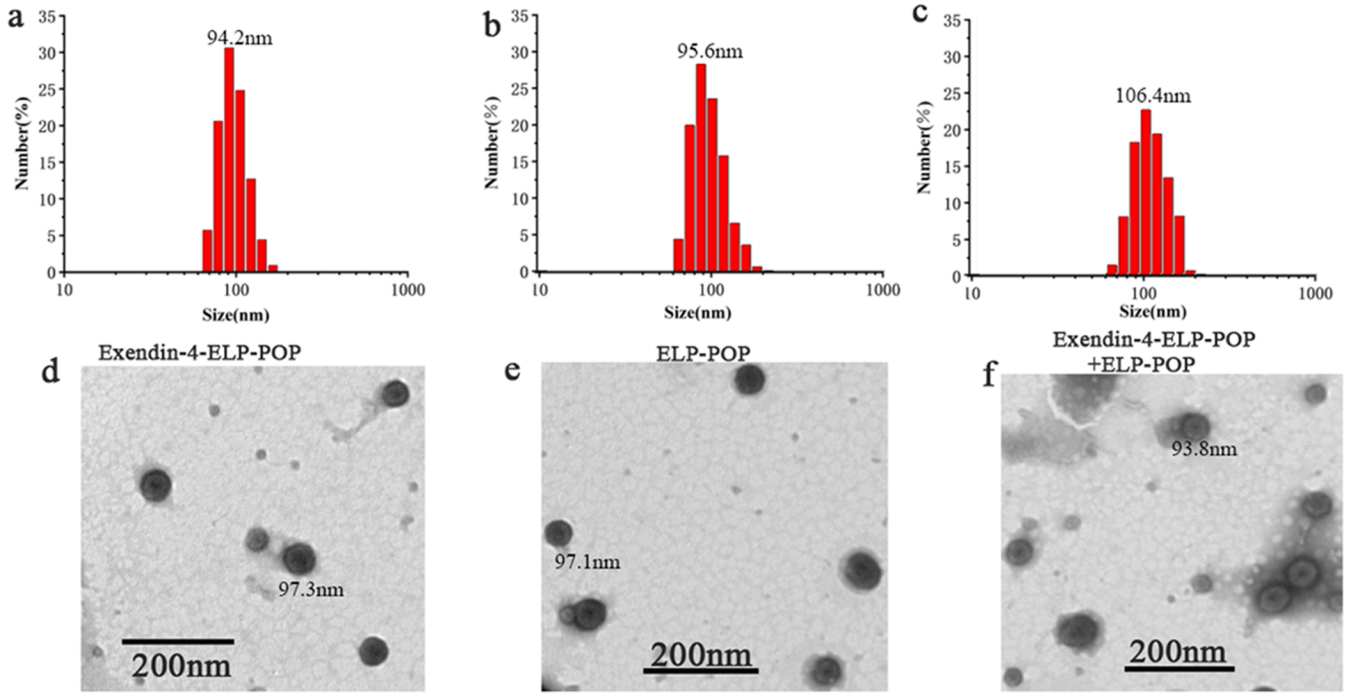

Figure 2. Diameter determination of ELP-POP nanoassemblies: the hydrated particle size of (a) Exendin-4-ELP-POP, (b) ELP-POP, and (c) combination of Exendin-4-ELP-POP with ELP-POP measured by DLS; TEM imaging for (d) Exendin-4-ELP-POP, (e) ELP-POP, and (f) combination of Exendin-4-ELP-POP with ELP-POP.

https://doi.org/10.1021/acsomega.3c04644
ACS Omega 2024, 9, 18757−18765

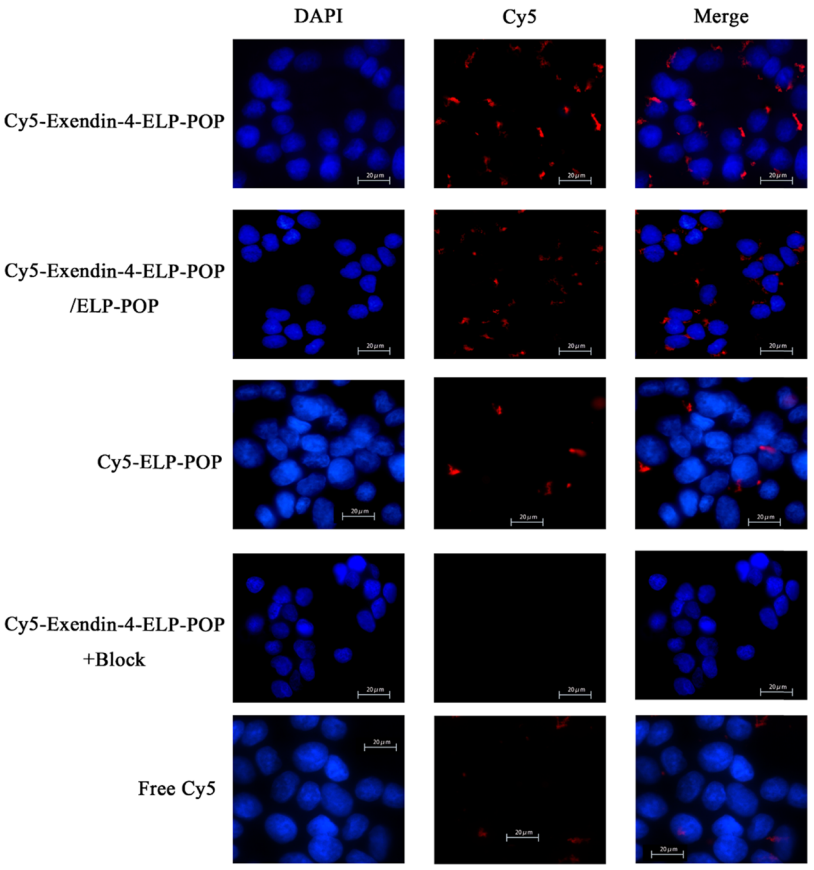

Figure 3. Fluorescence microscopy of Cy5-labeled Exendin-4-ELP-POP and ELP-POP incubated with INS-1 cells.

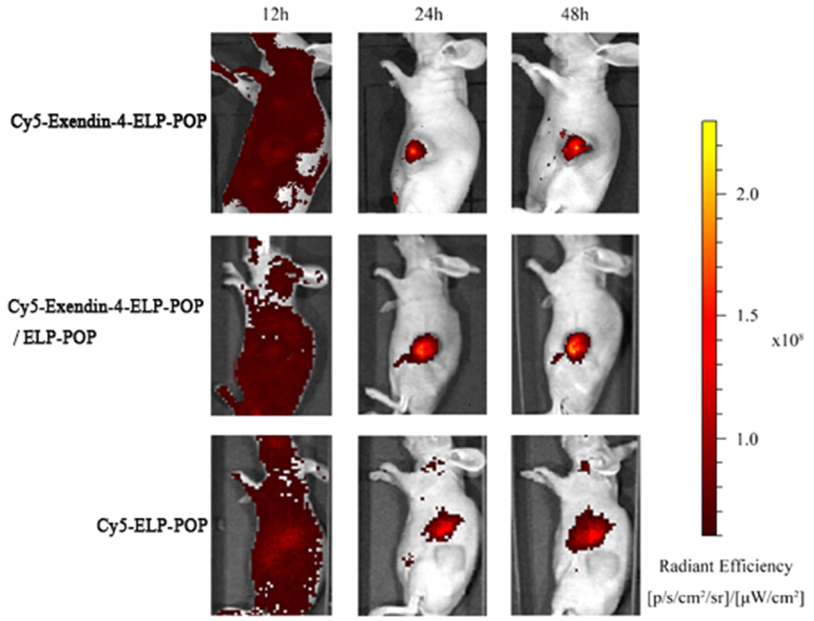

Figure 4. Fluorescence images of Cy5-labeled Exendin-4-ELP-POP and ELP-POP *in vivo*.

that the combination of Exendin-4-ELP-POP with Cy5-ELP-POP harbors similar affinity capability to Exendin-4-ELP-POP. Excessive Exendin-4 could block Cy5-Exendin-4-ELP-POP adsorption; this suggested that Exendin-4-ELP-POP and the combination of Exendin-4-ELP-POP with Cy5-ELP-POP targeted the GLP-1 receptor.[15]

3.4. *In Vitro* Cytotoxicity Assay. The cytotoxicity of ^{131}I-labeled ELP-POP and the combination of Exendin-4-ELP-POP with ELP-POP *in vitro* was tested. As shown in Figure S5, no significant cytotoxicity was observed in any of the test groups within the range of 1.85 MBq/mL. INS-1, which was treated with a 3.7 MBq/mL combination of Exendin-4-ELP-POP with ELP-POP, exhibited slight cell growth inhibition compared

https://doi.org/10.1021/acsomega.3c04644
ACS Omega 2024, 9, 18757−18765

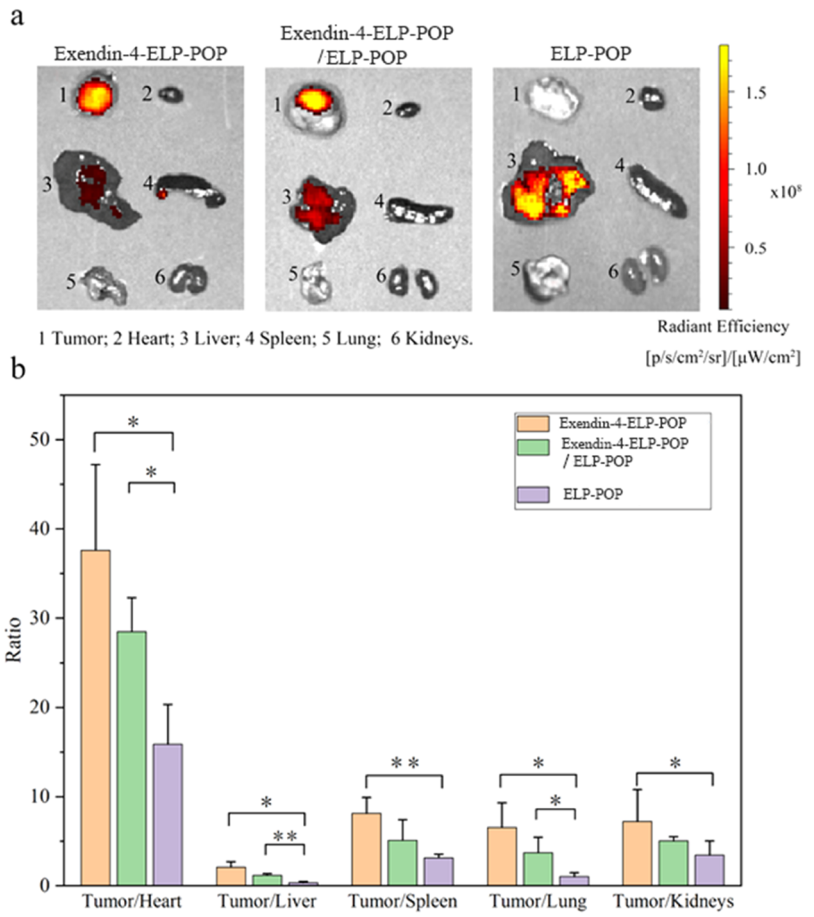

Figure 5. Fluorescence biodistribution of Cy5-labeled Exendin-4-ELP-POP and ELP-POP in insulinoma-bearing mice: (a) fluorescence images of different groups of tumors and representative organs *in vivo*; (b) ratio of tumor fluorescence intensity to organ fluorescence intensity in different groups (n = 3, *P < 0.05, **P < 0.01).

Table 1. Quantitative Analysis of the Imaging Intensity in the Tumor and Other Organs

unit [p/s/cm^2/sr]/[μW/cm^2]	tumor ×10^7	heart ×10^6	liver ×10^7	spleen ×10^7	lung ×10^7	kidney ×10^6
Exendin-4-ELP-POP	7.67 ± 1.65	2.04 ± 0.61	3.74 ± 0.26	9.45 ± 2.9	1.17 ± 0.51	1.06 ± 0.42
Exendin-4-ELP-POP/ELP-POP	6.14 ± 0.57	2.17 ± 0.82	6.35 ± 0.57	12.9 ± 3.7	1.67 ± 0.3	1.29 ± 0.43
ELP-POP	3.29 ± 0.64	2.46 ± 0.33	9.75 ± 1.2	9.78 ± 0.85	3.2 ± 0..88	0.96 ± 0.33

with the free ^{131}I, which may result from the higher affinity behavior between Exendin-4-ELP-POP/ELP-POP nanoassemblies.

3.5. *In Vivo* Real-Time Imaging. The tumor accumulation in insulinoma tumor-bearing nude mice was assessed after intravenous injection over time by near-infrared spectroscopy. Representative images are shown in Figure 4. Exendin-4-ELP-POP presented time-dependent tumor-targeting capability. As time elapsed, the fluorescent signal of Exendin-4-ELP-POP gradually increased at the tumor site. Our results suggested that Exendin-4-ELP-POP exhibited a higher tumor-affinity ability. In the case of the ELP-POP group, a remarkable fluorescent signal was primarily observed in the liver organ but appeared relatively faint in the tumor region 24 h post injection.

The combination of Cy5-Exendin-4-ELP-POP with ELP-POP group showed no remarkable intense fluorescent signal in the region of tumor within 12 h post injection. As time extended, an increasing fluorescent signal was detected at the tumor site compared with the normal tissues, indicating a similar outcome to the Exendin-4-ELP-POP group.

At 48 h post administration, the mice were immediately euthanized. The tumors and normal tissues were harvested for *ex vivo* imaging. The fluorescence image results of organs in each group are shown in Figure 5 and Table 1. In terms of the Cy5-Exendin-4-ELP-POP group, the average fluorescence intensity ratios of tumors to heart, liver, spleen, lung, and kidney were 37.60 ± 9.62, 2.06 ± 0.63, 8.12 ± 1.8, 6.53 ± 2.78, and 7.21 ± 3.59, respectively. The ratios of fluorescence intensity between the tumor and heart, liver, spleen, lung, and kidney in the combination of Cy5-Exendin-4-ELP-POP with ELP-POP group were 28.49 ± 3.81, 1.17 ± 0.18, 5.11 ± 2.30, 3.72 ± 1.70, and 5.04 ± 0.46, respectively. However, the fluorescence ratios of the Cy5-ELP-POP group to heart, liver, spleen, lung, and kidney were 15.87 ± 4.47, 0.33 ± 0.14, 3.14 ± 0.41, 1.02 ± 0.43, and 1.13 ± 1.60.

Noteworthily, the fluorescence intensity in the Cy5-Exendin-4-ELP-POP group was five times that of renal fluorescence intensity, which proved that Exendin-4-ELP-POP presented

https://doi.org/10.1021/acsomega.3c04644
ACS Omega 2024, 9, 18757−18765

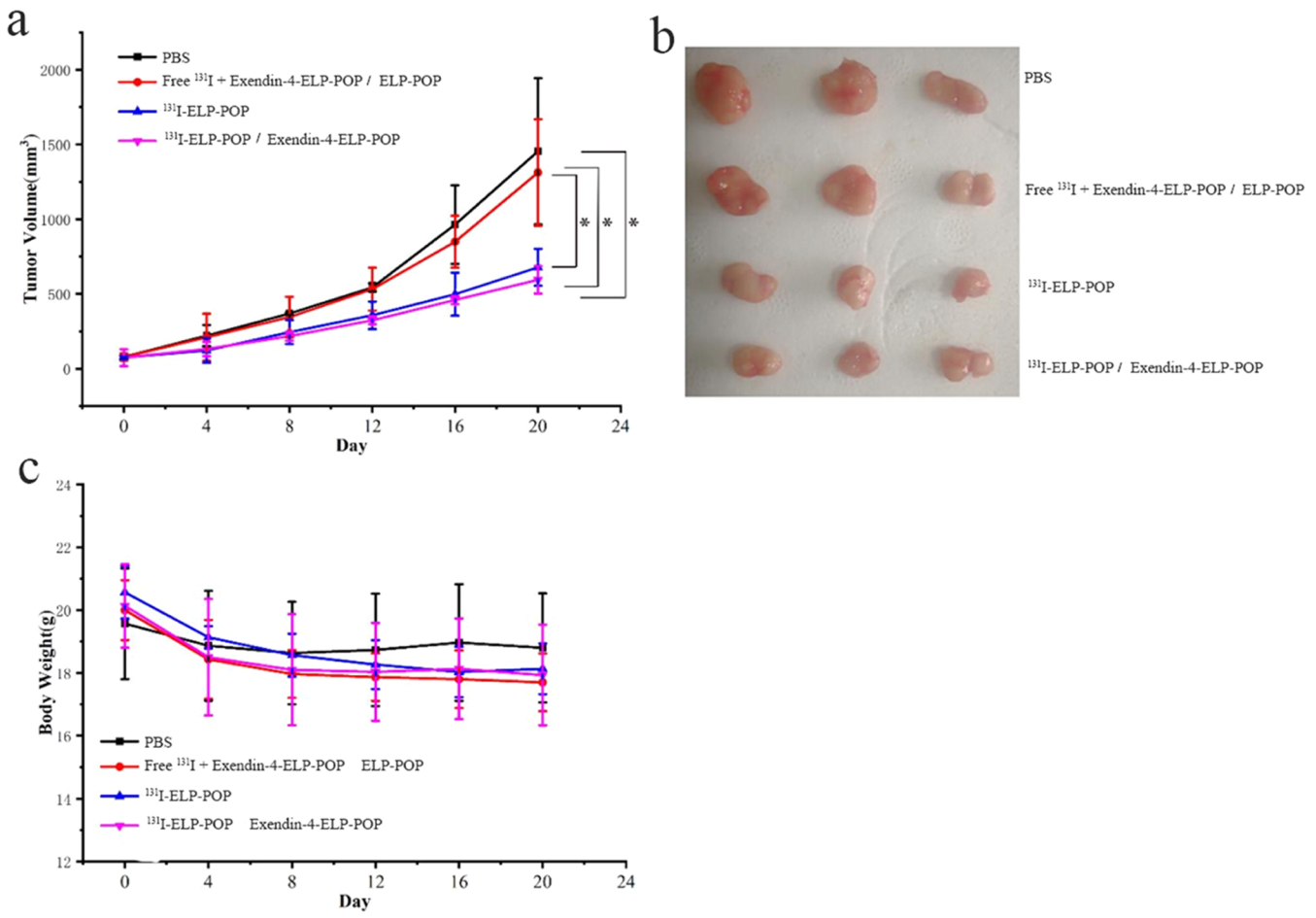

Figure 6. Effect of ^{131}I on tumor inhibition in insulinoma mice: (a) tumor growth curves of different groups of insulinoma model mice (n = 3, $^*P$ < 0.05); (b) body weight curves of different groups of insulinoma model mice (n = 3); and (c) physical images of tumors in different groups of insulinoma-bearing mice (n = 3).

less renal enrichment and higher insulinoma targeting ability. The combination of Cy5-Exendin-4-ELP-POP with ELP-POP group exhibited similar targeting capability to the Cy5-Exendin-4-ELP-POP group, with less enrichment in the kidney and more accumulation in the liver than the Cy5-Exendin-4-ELP-POP group. As for the fluorescence intensity of the Cy5-ELP-POP group, only a small deposition of fluorescent signals was observed in the tumor, while a higher intensity of fluorescent signals was detected in the liver.

3.6. Radiotherapeutic Effect *In Vivo*. After 18 h of dialysis (exchange with fresh PBS every 6 h), solution in the dialysis bag was harvested and the radioactive yield was 316.72 MBq. The labeling rate was calculated as 316.72 MBq/740 MBq × 100% = 41.3%.

To verify whether ^{131}I was successfully coupled with ELP-POP, we analyzed the molecular weights of ELP-POP and ^{131}I-ELP-POP by MAlDI-TOF. As shown in Figure S4, purity above 92% for ^{131}I-ELP-POP could be determined, and 14 ^{131}I molecules were conjugated per ELP-POP molecule.

The *in vivo* antitumor efficacy was assessed in mice bearing insulinomas. As shown in Figure 6, a single administration of free ^{131}I plus Exendin-4-ELP-POP and ELP-POP presented slight tumor growth suppression compared with the PBS control. In contrast, treatment with ^{131}I-ELP-POP and the combination of ^{131}I-ELP-POP with Exendin-4-ELP-POP at the same dosage achieved significantly higher tumor suppression effect. These results corroborated the remarkable tumor accumulation of ELP-POP and the combination of ELP-POP with Exendin-4-ELP-POP.

After the 20th administration, the tumor volume in the PBS group exceeded the limit standard according to the animal welfare guideline,[16] and the mice were anesthetized by inhalation, and the tumor tissue was harvested. As expected, tumor volume of the ^{131}I-ELP-POP and combination of ^{131}I-ELP-POP with Exendin-4-ELP-POP groups was 678 and 594 mm^3, respectively, compared with 1454 and 1312 mm^3, which point to the PBS and free ^{131}I plus Exendin-4-ELP-POP and ELP-POP groups.

As shown in Figure 6(c), the body weight in the PBS group showed no significant variation. However, the average weight loss in the free ^{131}I plus Exendin-4-ELP-POP and ELP-POP group was approximately 2 g, which may be attributed to the side effects of ^{131}I treatment. As shown in Figure S6, liver injury was not observed in any of the groups. These results preliminarily indicated that ^{131}I-ELP-POP exhibited an anti-insulinoma growth effect and low hepatotoxicity *in vivo*.

Hematoxylin−eosin staining (HE staining) displayed that less insulinoma cell apoptosis could be observed in the PBS and free ^{131}I plus Exendin-4-ELP-POP and ELP-POP groups. Apoptosis of a mass of cells could be detected in the ^{131}I-ELP-POP and combination of ^{131}I-ELP-POP with Exendin-4-ELP-POP groups (Figure S7).

https://doi.org/10.1021/acsomega.3c04644
ACS Omega 2024, 9, 18757−18765

4. DISCUSSION

GLP-1R is a G-protein-coupled receptor and overexpressed in organs such as the pancreas, intestine, lung, kidney, breast and brain and in pathological tissues such as insulinoma, gastrinoma, and pheochromocytoma, among which GLP-1R has the highest expression in insulinoma.[17] GLP-1R is one of the potential targets for tumor diagnosis and treatment, especially for the preoperative localization of insulinoma. In our previous study, conjugation of ^{68}Ga coupled with a GLP-1 analogue displayed excellent diagnostic effect for insulinoma. However, strong radionuclide radioactivity was observed in the kidney and bladder tissues,[3] whose radiation intensity was remarkably greater than that in the tumor tissues. As a result, they can bring about excessive radiation to the kidney or bladder. Furthermore, their clinical application is fairly restricted.

High kidney uptake interferes with the use of radiolabeled Exendin-4 derivatives in clinical practice. For example, [^{177}Lu]Lu-DO3A-VS-Cys40-Exendin-4 possessed outstanding targeting ability for insulinoma. Unfortunately, a dosimetry study displayed that the absorbed dose of [^{177}Lu]Lu-DO3A-VS-Cys40-Exendin-4 to kidneys limits the clinical application of the agent.[18] Several successful strategies to reduce the renal uptake of radiolabeled peptides have been exploited. Kaeppeli et al. demonstrated that the addition of an albumin-binding moiety to radiolabeled Exendin-4 results in a significant reduction of kidney uptake; chemical modification by an albumin-binding moiety could bring about more process complexity and affinity loss.[19] Joosten et al. developed [^{177}Lu]Lu-DOTA-MI-Exendin-4 and [^{68}Ga]Ga-NOTA-MI-Exendin-4 that showed reduced renal retention and improved tumor-to-kidney ratios; nevertheless, a methionine−isoleucine (MI) linker may be inclined to break.[20] In terms of our preparation method, the strategy of an Exendin-4 block fused with ELP and POP could abolish chemical coupling and enhance agent stability.

ELP and its analogues POP harbor biocompatibility behavior, and their amino acid composition could be precisely controlled by genetic coding, thus improving the half-life and biodistribution of drug preparations.[21] The amphiphilic ELP nanoassembly formation was driven by the hydrophobic effect.[9,10] In this study, we designed Exendin-4-ELP-POP with the ability to target GLP-1R and ELP-POP with multiple radioiodine conjugation sites via genetic engineering. Our results showed that Exendin-4-ELP-POP formed spherical nanoassemblies. The *in vitro* fluorescence study demonstrated that Exendin-4-ELP-POP clustered around the insulinoma cell membrane. The combination of Cy5-Exendin-4-ELP-POP with ELP-POP also exhibited targeting capability similar to that of Exendin-4-ELP-POP. *In vivo* imaging results showed that the combination of Exendin-4-ELP-POP and ELP-POP also exhibited similar targeting capability to Exendin-4-ELP-POP. Compared with ^{68}Ga-Exendin-4, the combination of Exendin-4-ELP-POP with ELP-POP can form ∼100 nm nanoassemblies, which can effectively reduce glomerular filtration, and avoid the accumulation of the nanoassemblies in the kidney tumor, thereby reducing the toxicity to the kidney and bladder.[22] *Ex vivo* fluorescence imaging analysis showed that the fluorescence intensity of the liver was significantly higher in the ELP-POP group except for the tumor because the liver acts as a biological metabolic system and sequesters most of the administered nanoassemblies from the bloodstream.[23]

The combination of radiation isotopes with ELPs had been used in brachytherapy to radiate tumors;[24] this approach avoided the traditional brachytherapy implantation procedure. ^{131}I can generate highly active β-particle emission and has been widely used in tumor radiotherapy.[24,25] The recombinant fusion protein ELP-POP designed in this study contained multiple tyrosine residues that could conjugate ^{131}I. ELP-POP was labeled with ^{131}I by iodination, and then the combination with Exendin-4-ELP-POP formed spherical nanoassemblies under physiological conditions. Our results demonstrated that the combination of ^{131}I-labeled ELP-POP and Exendin-4-ELP-POP achieved favorable inhibitory effect on insulinoma.

5. CONCLUSIONS

In summary, we designed a ternary block recombinant protein that could self-assemble into a nanoscale formulation. The nanoscale formulation was capable of achieving a high radionuclide load and demonstrated an outstanding affinity for insulinoma cells. Intravenous injection of the nanoscale formulation, specifically a combination of ^{131}I-ELP-POP and Exendin-4-ELP-POP, induced significant tumor regression in a tumor xenograft model. Our research suggests the potential application of the nanoscale formulation as a safe and efficient strategy for treating insulinoma.

■ ASSOCIATED CONTENT

Supporting Information

The Supporting Information is available free of charge at https://pubs.acs.org/doi/10.1021/acsomega.3c04644.

Identification of plasmids pET-23a-ELP-POP and pET-23a-Exendin-4-ELP-POP; determination of the phase transition temperature of Exendin-4-ELP-POP and ELP-POP; *in vitro* imaging of Exendin-4-ELP-POP nanoassemblies; protein identified by MALDI-TOF; *in vitro* cytotoxicity analysis; liver injury determination; and tumor therapeutic evaluation in vivo (PDF)

■ AUTHOR INFORMATION

Corresponding Authors

Hongwei Fan − *Department of Clinical Pharmacology Lab, Nanjing First Hospital, Nanjing Medical University, Nanjing 210006, P. R. China; School of Basic Medicine and Clinical Pharmacy, China Pharmaceutical University, Nanjing 210009, P. R. China*; Phone: +86-025-52271448; Email: fanhongwei178@sina.com

Jianjun Zou − *Department of Clinical Pharmacology Lab, Nanjing First Hospital, Nanjing Medical University, Nanjing 210006, P. R. China; School of Basic Medicine and Clinical Pharmacy, China Pharmaceutical University, Nanjing 210009, P. R. China*; Phone: +86-025-52271448; Email: zoujianjun100@126.com

Kaizong Huang − *Department of Clinical Pharmacology Lab, Nanjing First Hospital, Nanjing Medical University, Nanjing 210006, P. R. China*; orcid.org/0000-0002-4926-6980; Phone: +86-025-52271448; Email: kzhuang@nju.edu.cn

Authors

Zhengwei Zhou − *Department of Clinical Pharmacology Lab, Nanjing First Hospital, Nanjing Medical University, Nanjing 210006, P. R. China; School of Basic Medicine and Clinical*

https://doi.org/10.1021/acsomega.3c04644
ACS Omega 2024, 9, 18757−18765

Pharmacy, China Pharmaceutical University, Nanjing 210009, P. R. China

Shuai Wang − *Department of Clinical Pharmacology Lab, Nanjing First Hospital, Nanjing Medical University, Nanjing 210006, P. R. China; School of Basic Medicine and Clinical Pharmacy, China Pharmaceutical University, Nanjing 210009, P. R. China*

Tianling Feng − *Department of Clinical Pharmacology Lab, Nanjing First Hospital, Nanjing Medical University, Nanjing 210006, P. R. China; School of Basic Medicine and Clinical Pharmacy, China Pharmaceutical University, Nanjing 210009, P. R. China*

Pengjun Zhang − *Department of Nuclear Medicine, Nanjing First Hospital, Nanjing Medical University, Nanjing 210006, P. R. China*

Complete contact information is available at: https://pubs.acs.org/10.1021/acsomega.3c04644

Notes

All animal experiments were approved by the Institutional Animal Ethics Committee of Nanjing Medical University affiliated to Nanjing First Hospital (DWSY-1901222). In addition, all institutional and national guidelines for the care and use of animals were followed.

The authors declare no competing financial interest.

■ ACKNOWLEDGMENTS

This study received the following financial support: the National Natural Science Foundation of China Grants (No. 81673511), Open project of International Joint Laboratory of Recombinant Drug Protein Expression System in Henan Province (No. KFKTYB202208), Jiangsu key Research Development Plan Grant (No. BE2017613), and the Natural Science Foundation of Jiangsu Province (No. BK20190131). We would like to thank Editage (www.editage.cn) for English language editing.

■ REFERENCES

(1) Murakami, T.; Fujimoto, H.; Inagaki, N. Non-invasive Beta-cell Imaging: Visualization, Quantification, and Beyond. *Front. Endocrinol.* **2021**, *12*, No. 714348.

(2) Christ, E.; Antwi, K.; Fani, M.; Wild, D. Innovative imaging of insulinoma: the end of sampling? A review. *Endocr.-Relat. Cancer* **2020**, *27* (4), R79−R92.

(3) Zhang, P.; Zhao, Z.; Zhang, L.; Wu, W.; Xu, Y.; Pan, D.; Wang, F.; Yang, M. [Ga]Ga-NOTA-MAL-Cys-exendin-4, a potential GLP-1R targeted PET tracer for the detection of insulinoma. *Nucl. Med. Biol.* **2019**, *74-75*, 19−24.

(4) Iikuni, S.; Kamei, I.; Ohara, T.; Watanabe, H.; Ono, M. Development of an In-Labeled Glucagon-Like Peptide-1 Receptor-Targeting Exendin-4 Derivative that Exhibits Reduced Renal Uptake. *Mol. Pharmaceutics* **2022**, *19* (3), 1019−1027.

(5) Zhang, M.; Jacobson, O.; Kiesewetter, D.; Ma, Y.; Wang, Z.; Lang, L.; Tang, L.; Kang, F.; Deng, H.; Yang, W.; et al. Improving the Theranostic Potential of Exendin 4 by Reducing the Renal Radioactivity through Brush Border Membrane Enzyme-Mediated Degradation. *Bioconjugate Chem.* **2019**, *30* (6), 1745−1753.

(6) Li, H.; Sun, J.; Zhu, H.; Wu, H.; Zhang, H.; Gu, Z.; Luo, K. Recent advances in development of dendritic polymer-based nanomedicines for cancer diagnosis. *WIREs Nanomed. Nanobiotechnol.* **2021**, *13* (2), No. e1670.

(7) Gu, L.; Duan, Z.; Li, X.; Li, X.; Li, Y.; Li, X.; Xu, G.; Gao, P.; Zhang, H.; Gu, Z.; et al. Enzyme-triggered deep tumor penetration of a dual-drug nanomedicine enables an enhanced cancer combination therapy. *Bioact. Mater.* **2023**, *26*, 102−115.

(8) American Diabetes Association. 2. Classification and Diagnosis of Diabetes: Standards of Medical Care in Diabetes-2019. *Diabetes care* **2019**, *42*, S13−S28.

(9) Huang, K.; Gao, M.; Fan, L.; Lai, Y.; Fan, H.; Hua, Z. IR820 covalently linked with self-assembled polypeptide for photothermal therapy applications in cancer. *Biomater. Sci.* **2018**, *6* (11), 2925−2931.

(10) Huang, K.; Zhu, L.; Wang, Y.; Mo, R.; Hua, Z. Targeted delivery and release of doxorubicin using a pH-responsive and self-assembling copolymer. *J. Mater. Chem. B* **2017**, *5* (31), 6356−6365.

(11) Roberts, S.; Miao, V.; Costa, S.; Simon, J.; Kelly, G.; Shah, T.; Zauscher, S.; Chilkoti, A. Complex microparticle architectures from stimuli-responsive intrinsically disordered proteins. *Nat. Commun.* **2020**, *11* (1), No. 1342. Roberts, S.; Harmon, T.; Schaal, J.; Miao, V.; Li, K.; Hunt, A.; Wen, Y.; Oas, T.; Collier, J.; Pappu, R.; Chilkoti, A. Injectable tissue integrating networks from recombinant polypeptides with tunable order. *Nat. Mater.* **2018**, *17* (12), 1154−1163.

(12) Etrych, T.; Subr, V.; Strohalm, J.; Sírová, M.; Ríhová, B.; Ulbrich, K. HPMA copolymer-doxorubicin conjugates: The effects of molecular weight and architecture on biodistribution and in vivo activity. *J. Controlled Release* **2012**, *164* (3), 346−354.

(13) Lo, W.-L.; Wang, Y.-H.; Chen, E. H. L.; Wang, S.-M.; Chen, L.-C.; Chen, R. P. Y. Biodistribution analysis of an intranasal-delivered peptide by the nanoSPECT/CT imaging. *J. Drug Delivery Sci. Technol.* **2022**, *73*, No. 103454.

(14) Liu, J.; Zhang, Y.; Li, Q.; Feng, Z.; Huang, P.; Wang, W.; Liu, J. Development of injectable thermosensitive polypeptide hydrogel as facile radioisotope and radiosensitizer hotspot for synergistic brachytherapy. *Acta Biomater.* **2020**, *114*, 133−145.

(15) Kiesewetter, D. O.; Guo, N.; Guo, J.; Gao, H.; Zhu, L.; Ma, Y.; Niu, G.; Chen, X. Evaluation of an [(18)F]AlF-NOTA Analog of Exendin-4 for Imaging of GLP-1 Receptor in Insulinoma. *Theranostics* **2012**, *2* (10), 999−1009. Kim Chung, L. T.; Hosaka, T.; Yoshida, M.; Harada, N.; Sakaue, H.; Sakai, T.; Nakaya, Y. Exendin-4, a GLP-1 receptor agonist, directly induces adiponectin expression through protein kinase A pathway and prevents inflammatory adipokine expression. *Biochem. Biophys. Res. Commun.* **2009**, *390* (3), 613−618.

(16) Mezencev, R.; McDonald, J. Subcutenous xenografts of human T-lineage acute lymphoblastic leukemia Jurkat cells in nude mice. *In vivo* **2011**, *25* (4), 603−607. Couturier, D.-L.; Bertrand, H. Animal number versus maximum tumour volume: an example of reduction and refinement trade-off in the 3Rs. *Lab. Anim.* **2022**, *51* (8), 208−209.

(17) Wang, P.; Yoo, B.; Yang, J.; Zhang, X.; Ross, A.; Pantazopoulos, P.; Dai, G.; Moore, A. GLP-1R-targeting magnetic nanoparticles for pancreatic islet imaging. *Diabetes* **2014**, *63* (5), 1465−1474. Körner, M.; Christ, E.; Wild, D.; Reubi, J. Glucagon-like peptide-1 receptor overexpression in cancer and its impact on clinical applications. *Front. Endocrinol.* **2012**, *3*, 158.

(18) Velikyan, I.; Bulenga, T. N.; Selvaraju, R.; Lubberink, M.; Espes, D.; Rosenström, U.; Eriksson, O. Dosimetry of [(177)Lu]-DO3A-VS-Cys(40)-Exendin-4 - impact on the feasibility of insulinoma internal radiotherapy. *Am. J. Nucl. Med. Mol. Imaging* **2015**, *5* (2), 109−126. From NLM.

(19) Kaeppeli, S. A. M.; Jodal, A.; Gotthardt, M.; Schibli, R.; Béhé, M. Exendin-4 Derivatives with an Albumin-Binding Moiety Show Decreased Renal Retention and Improved GLP-1 Receptor Targeting. *Mol. Pharmaceutics* **2019**, *16* (9), 3760−3769.

(20) Joosten, L.; Frielink, C.; Jansen, T.; Lobeek, D.; Andreae, F.; Konijnenberg, M.; Heskamp, S.; Gotthardt, M.; Brom, M. New Radiolabeled Exendin Analogues Show Reduced Renal Retention. *Mol. Pharmaceutics* **2023**, *20* (7), 3519−3528.

(21) Milligan, J. J.; Saha, S.; Jenkins, I.; Chilkoti, A. Genetically encoded elastin-like polypeptide nanoparticles for drug delivery. *Curr. Opin. Biotechnol.* **2022**, *74*, 146−153. Jenkins, I. C.; Milligan, J.; Chilkoti, A. Genetically Encoded Elastin-Like Polypeptides for Drug Delivery. *Adv. Healthcare Mater.* **2021**, *10* (13), No. e2100209. Varanko, A. K.; Su, J.; Chilkoti, A. Elastin-Like Polypeptides for Biomedical Applications. *Annu. Rev. Biomed. Eng.* **2020**, *22*, 343−369.

(22) Weiner, I. D.; Verlander, J. Renal ammonia metabolism and transport. *Compr. Physiol.* **2011**, *3* (1), 201−220.
(23) Tang, Y.; Wang, X.; Li, J.; Nie, Y.; Liao, G.; Yu, Y.; Li, C. Overcoming the Reticuloendothelial System Barrier to Drug Delivery with a ″Don't-Eat-Us″ Strategy. *ACS Nano* **2019**, *13* (11), 13015−13026. Zhang, Y.-N.; Poon, W.; Tavares, A.; McGilvray, I.; Chan, W. Nanoparticle-liver interactions: Cellular uptake and hepatobiliary elimination. *J. Controlled Release* **2016**, *240*, 332−348.
(24) Sun, N.; Zhao, L.; Zhu, J.; Li, Y.; Song, N.; Xing, Y.; Qiao, W.; Huang, H.; Zhao, J. I-labeled polyethylenimine-entrapped gold nanoparticles for targeted tumor SPECT/CT imaging and radionuclide therapy. *Int. J. Nanomed.* **2019**, *14*, 4367−4381.
(25) Zhao, L.; Zhu, J.; Cheng, Y.; Xiong, Z.; Tang, Y.; Guo, L.; Shi, X.; Zhao, J. Chlorotoxin-Conjugated Multifunctional Dendrimers Labeled with Radionuclide 131I for Single Photon Emission Computed Tomography Imaging and Radiotherapy of Gliomas. *ACS Appl. Mater. Interfaces* **2015**, *7* (35), 19798−19808.

https://doi.org/10.1021/acsomega.3c04644
ACS Omega 2024, 9, 18757−18765